NUMERICAL STUDIES IN NON-OHMIC HOPPING CONDUCTION IN RANDOM SYSTEMS

JAROSŁAW RYBICKI and GIORGIO MANCINI[#]

Department of Solid State Physics,
Faculty of Technical Physics and Applied Mathematics,
Technical University of Gdańsk, Narutowicza 11/12, 80-954 Gdańsk, Poland
and
Academic Computer Centre of Gdańsk,
Narutowicza 11/12, 80-954 Gdańsk, Poland
ryba@pg.gda.pl
[#]*Istituto di Matematica e Fisica, Universita' di Camerino,*
via Madonna delle Carceri, Camerino (MC), Italy
mancini@task.gda.pl

Abstract: Phonon-assisted hopping of carriers between spatially distinct locations is the basic transport mechanisms in low-mobility solids (weakly doped or strongly compensated semiconductors, amorphous solids, glasses, organic solids, transition metal oxides, superionic conductors). In the present paper we consider the electron transport close to the Fermi level. The calculation of the current-field characteristics in random hopping systems for arbitrary strength of the electric field is a rather complicated task. It involves simplified methods such as percolation theory or effective medium approximation (EMA), or requires a purely numerical treatment. A short review of our recent work within the letter approach is presented below. In particular, we discuss the dependence of the current-field, and differential conductivity-field characteristics on: 1) the amount of the off-diagonal disorder; 2) the system dilution; 3) the degree of the macroscopic-scale spatial non-uniformity of the hopping centre density.

1. Introduction

Phonon-assisted hopping of particles between spatially distinct locations is one of the basic transport mechanisms in solids [1-3]. The hopping mechanism dominates in low-mobility systems. In particular, the mechanism is active in a great variety of materials such as weakly doped or strongly compensated semiconductors, amorphous solids, glasses, organic solids, transition metal oxides, superionic conductors. In the present work we concentrate ourselves on the electron transport close to the Fermi level.

A theoretical study of the charge carrier hopping transport starts from a model Hamiltonian that takes into account all the essential features of the specific system.

The Hamiltonian must describe electron subsystem, phonon subsystem, electron-phonon interaction, and the interaction with external fields. The electric current can be expressed by the diagonal elements of the density matrix. In the case of hopping at the Fermi level the one-electron approximation is obviously not sufficient, and at least the Hartree-Fock decoupling should be performed in order to get the proper density matrix equation of motion. For crystalline systems, because of their translational symmetry, a great deal of analytical work can be done. On the other hand, the calculation of the current-field characteristics in random hopping systems involves simplified methods such as percolation theory [4-9] or effective medium approximation (EMA) [10-12], or requires a purely numerical treatment [13-18]. A short review of our recent [18] work within the letter approach is presented below.

The paper is organised as follows. In Section 2 the electron hopping problem is formulated, and the general physical theory of this section is translated to the numerical problem in Section 3. Some exemplary results are presented and discussed in Section 4. Section 5 contains concluding remarks.

2. General formalism

It is assumed [1], that electron transitions between different levels of an atom do not effect the charge transport. Consequently, each atom is assumed to have only a single energy level. The one-electron wave function, $\Psi(\mathbf{r})$, is written as a superposition of the atomic electron wave functions φ_m:

$$\Psi(\mathbf{r}) = \sum_m a_m \varphi_m(\mathbf{r}-\mathbf{R}) , \tag{1}$$

where $\varphi_m(\mathbf{r}-\mathbf{R}_m)$ is the solution of:

$$\left[\frac{-\hbar^2}{2m_e}\Delta + U_m(\mathbf{r}-\mathbf{R}_m) \right] \varphi_m(\mathbf{r}-\mathbf{R}_m) = \varepsilon_m \varphi_m(\mathbf{r}-\mathbf{R}_m) . \tag{2}$$

Here $U_m(\mathbf{r}-\mathbf{R}_m)$ is the electron potential at the m-th atom located at $\mathbf{R}_m$, m_e is the mass of the electron, and Δ is the Laplace operator.

2.1. Hamiltonian

As mentioned in the introduction the full Hamiltonian H suitable for the study of the hopping transport contains components describing electron subsystem H_e, phonon subsystem H_{ph}, electron-phonon interaction $H_{e\text{-}ph}$, and interactions with the external electric field H_E. In particular, the Hamiltonian components are constructed as follows:

a) electron subsystem Hamiltonian,

$$H_e = \sum_m \varepsilon_m a_m^+ a_m + \sum_{m'm} J_{m'm} a_{m'}^+ a_m , \tag{3}$$

where a_m^+ and a_m are the creation and annihilation operators of the electron in the state $\varphi_m(\mathbf{r}-\mathbf{R}_m)$, respectively, ε_m is the electronic energy of the m-th atom, and $J_{m'm}$ is the resonance integral between the neighbouring sites:

$$\varepsilon_m = \langle \varphi_m(\mathbf{r}-\mathbf{R}_m)|H_e|\varphi_m(\mathbf{r}-\mathbf{R}_m)\rangle ,$$

$$J_{m'm} = \langle \varphi_{m'}(\mathbf{r}-\mathbf{R}_{m'})|H_e|\varphi_m(\mathbf{r}-\mathbf{R}_m)\rangle ; \tag{4}$$

b) phonon subsystem Hamiltonian,

$$H_{ph} = \hbar\omega_{\mathbf{q}}(b_{\mathbf{q}}^+ b_{\mathbf{q}} + 1/2) , \tag{5}$$

where $\omega_{\mathbf{q}}$ is the frequency of the phonon with the wave vector $\mathbf{q}$, whereas $b_{\mathbf{q}}^+$, and $b_{\mathbf{q}}$ are the phonon creation, and annihilation operators, respectively;

c) electron-phonon interaction,

$$H_{e-ph} = \sum_{m,\mathbf{q}} a_m^+ a_m \hbar\omega_{\mathbf{q}} \left[u_m(\mathbf{q}) b_{\mathbf{q}} + u_m^*(\mathbf{q}) b_{\mathbf{q}}^+\right] , \tag{6}$$

where

$$u_m(\mathbf{q}) = \frac{1}{\sqrt{2N}} \gamma_m(\mathbf{q}) \exp(-i\mathbf{q}\mathbf{R}_m) , \tag{7}$$

and $\gamma_m(\mathbf{q})$ is the electron-phonon coupling constant, and N is the total number of sites in the system;

d) interaction with external electric field,

$$H_E = -\mathbf{D}\mathbf{E} , \tag{8}$$

where $\mathbf{D}$ is the operator of the dipole moment,

$$\mathbf{D} = e\sum_{m,m'} \mathbf{d}_{m'm}\, a_m^+ a_m, \qquad \mathbf{d}_{m'm} = \langle \varphi_{m'}(\mathbf{r}-\mathbf{R})_{m'}|\mathbf{r}|\varphi_m(\mathbf{r}-\mathbf{R}_m)\rangle , \tag{9}$$

and e is the electron charge.

The total Hamiltonian for the hopping system is the sum of the above contributions:

$$H = H_e + H_{ph} + H_{e-ph} + H_E . \tag{10}$$

In amorphous materials $\mathbf{R}_m$, ε_m and $J_{m'm}$ (4) are random variables, and $\varphi_m(\mathbf{r}-\mathbf{R}_m)$ is interpreted as a localised state centred at $\mathbf{R}_m$.

2.2. Electric current

The electric current $\mathbf{j}$ is related to the dipole moment $\mathbf{D}$ by the expression

$$\mathbf{j}(t) = \frac{1}{\Omega}\frac{d\,\mathbf{D}(t)}{dt} , \tag{11}$$

where Ω is the volume of the system, and

$$\mathbf{D}(t) = U^{+}(t)\ \mathbf{D}\ U(t)\,, \tag{12}$$

with the time-evolution operator

$$U(t) = \exp\Big[-\frac{i}{\hbar}\int_0^t H(t')dt'\Big]\,. \tag{13}$$

Approximating **D** by

$$\mathbf{D} = e\sum_m \mathbf{R}_m\, a_m^{+} a_m\,, \tag{14}$$

which corresponds to the neglecting of the non-diagonal elements in respect to the site indices, one obtains

$$\mathbf{j}\,(t) = \frac{e}{\Omega}\sum_m \mathbf{R}_m \frac{d\rho_m(t)}{dt}\,, \tag{15}$$

where ρ_m is the m-th diagonal element of the density matrix, and describes the thermodynamically averaged concentration of the charge carriers at the m-th hopping centre. The average concentrations ρ_m are given by [1]

$$\rho_m(t) = \frac{Tr\left\{e^{-(H^{(0)}-\mu\hat{N})/kT}U^{+}(t)a_m^{+}a_m U(t)\right\}}{Tr\left\{e^{-(H^{(0)}-\mu\hat{N})/kT}\right\}}\,, \tag{16}$$

where μ is the chemical potential, and $\hat{N}$ is the particle number operator, $\hat{N} = \sum_m a_m^{+} a_m$, and in the Markovian limit obey:

$$\frac{d\rho_m(t)}{dt} = \sum_{m'}\left\{\rho_{m'}(t)(1-\rho_m(t))W_{m'm}(t) - \rho_m(t)(1-\rho_{m'}(t))W_{mm'}(t)\right\} \tag{17}$$

where $W_{m'm}$ are the symmetrised jump probabilities.

3. Numerical model for the dc conductivity

The bulk density of the dc hopping current is given by

$$\mathbf{j} = \frac{1}{2\Omega}\sum_{m,m'}(\mathbf{R}_m - \mathbf{R}_{m'})\cdot i(m',m)\,, \tag{18}$$

where

$$i(m',m) = eW_{m'm}\Big[\rho_{m'}(1-\rho_m)\exp(\beta V_{m'm}/2) - \rho_m(1-\rho_{m'})\exp(-\beta V_{m'm}/2)\Big]\,. \tag{19}$$

Here $V_{m'm} = V_{m'} - V_m$, $V_m = \rho_m + eu_m$, where ρ_m is the energy of the m-th centre, u_m is the external field potential at the point $\mathbf{R}_m$, $\beta = kT$, ρ_m is the occupation probability of the m-th centre, and $W_{m'm}$ is the symmetrised jump probability [1]:

$$W_{m'm} = \int_{-\infty}^{\infty} dt' \cos(V_{m'm}t'/\hbar)\varphi_{m'm}(t') \,, \tag{20}$$

$$\varphi_{m'm}(t) = \hbar^{-2}|J_{m'm}|^2 \exp(-2S_I(m', m))\times$$

$$\times\left\{\exp\left[\sum_{\mathbf{q}} \frac{|\gamma(\mathbf{q})|^2[1-\cos(\mathbf{q}(\mathbf{R}_{m'}-\mathbf{R}_m))]}{N\sinh(\hbar\omega_{\mathbf{q}}\beta/2)}\cos\omega_{\mathbf{q}}t\right]-1\right\}, \tag{21}$$

$$S_I(m',m) = \frac{1}{2N}\sum_{\mathbf{q}} |\gamma(\mathbf{q})|^2\left[1-\cos(\mathbf{q}(\mathbf{R}_{m'}-\mathbf{R}_m))\right]\coth(\hbar\omega_{\mathbf{q}}\beta/2) \,. \tag{22}$$

In the limit of strong electron-phonon interaction, $|\gamma(\mathbf{q})|^2 >> 1$, the expression for $W_{mm'}$ is dominated by the square of the resonance integral,

$$W_{m'm} = W_0 \cdot \exp(-2\alpha|\mathbf{R}_{m'm}|) \,. \tag{23}$$

where W_0 weakly depends on the external field, if only $e\mathbf{E}(\mathbf{R}_{m'}-\mathbf{R}_m)_x$ is smaller then a typical barrier height between the centres m and m'.

For each centre m, $m = 1,..., N$, the Kirchhoff law applies,

$$\sum_{m'} i(m',m) = 0 \,, \tag{24}$$

where suitable periodic boundary conditions must be taken into account. The above system of equations is being solved numerically under the following normalisation condition:

$$N^{-1}\sum_{m} \rho_m = n \,, \tag{25}$$

where N is the total number of localised states in volume, and n is the average electron concentration.

The algorithm can be summarised as follows. Let $\rho_1,...,\rho_r$ denote the occupation probabilities of the centres belonging to the contacts, and $\rho_{r+1},..., \rho_N$ - occupation probabilities of the bulk centres. According to the model the following system of equations is obeyed:

$$F_1(\rho) = \sum_{m'=1}^{N} \rho_{m'} - Nn = 0 \,, \tag{26}$$

$$F_m(\rho) = \rho_{m-1}(1-\rho_m)\exp(-\beta\varepsilon_m) - \\ -\rho_m(1-\rho_{m-1})\exp(-\beta\varepsilon_{m-1}) = 0\,, \qquad m = 2, \ldots, r \tag{27}$$

$$F_m(\rho) = \sum_{m'=1}^{N} W_{m'm}\,[\rho_{m'}(1-\rho_m)\exp(\beta V_{m'm}/2) - \\ -\rho_m(1-\rho_{m'})\exp(-\beta V_{m'm}/2)] = 0\,, \qquad m = r+1, \ldots N, \tag{28}$$

where $\rho = [\rho_1, \rho_2, \ldots, \rho_N]^T$. Equations (26)-(28) are solved using the following iteration procedure:

$$\rho^{(k+1)} = \rho^k - \lambda_k \left[\frac{\partial F(\rho)}{\partial \rho} \Big|_{\rho^{(0)}} \right]^{-1} F(\rho^{(k)})\,, \qquad k = 1,2,\ldots, \tag{29}$$

where k denotes the number of the successive iteration, and $F(\rho) = [F_1(\rho), F_2(\rho), \ldots, F_N(\rho)]^T$. The algorithm has been highly optimised [16] taking advantage of a partial sparseness of the matrix

$$\left[\frac{\partial F(\rho)}{\partial \rho} \Big|_{\rho(0)} \right]^{-1},$$

due to a particular form of the equations for the near-contact centres. Both singular decomposition and Gauss elimination methods were applied. After calculations within the modified Newton relaxation method several iterations with the standard Newton method ($l = 1$) were performed. On this stage the norm of the functional F was being controlled, and so the best result was accepted. Finally, the solution of the system

$$\frac{d\rho(E)}{dE} = -\left[\frac{\partial F(\rho)}{\partial \rho} \Big|_{\rho(0)} \right]^{-1} \frac{\partial F}{\partial E}$$

was being corrected by iterative relaxation methods. Our modifications of the original Bottger and Bryksin algorithm [13] allowed a significant increase of the solution accuracy. The CPU time necessary to calculate one j-E characteristic for 1000 centres in the simulation box was 4-6 hours on the SGI workstation with the R10000 processor.

For hopping systems with a translational symmetry, the j-E characteristics can be calculated almost analytically. In particular, the small polaron transport can be described starting from the equation

$$\frac{d\rho_m(t)}{dt} = \sum_{m'} \left[\rho_{m'}(t) W_{m'm}(t) - \rho_m(t) W_{mm'}(t) \right] . \tag{30}$$

In the case of time-independent electric fields, the $W_{mm'}$ coefficients are constant, and the Laplace transform of (30) reads:

$$s\rho_m(s) = f_m + \sum_{m'} \left[\rho_{m'}(s) W_{m'm} - \rho_m(s) W_{mm'} \right] , \tag{31}$$

where $f_m = \rho_m(t)|_{t=0}$. Taking now the Fourier transform we get from (31)

$$\rho(\mathbf{k},s) = f(\mathbf{k}) \,/ \left[s + W(0) - W(\mathbf{k}) \right] \tag{32}$$

where:

$$\rho(\mathbf{k},s) = \sum_m \rho_m(s) \exp(i\mathbf{k}\mathbf{R}_m) , \tag{33}$$

$$W(\mathbf{k}) = \sum_m W_{m',m+m'} \exp(i\mathbf{k}\mathbf{R}_m) , \tag{34}$$

$$f(\mathbf{k}) = \sum_m f_m \exp(i\mathbf{k}\mathbf{R}_m) . \tag{35}$$

On the other hand the general expression for the current density (15), submitted to the Laplace and Fourier transformations, after taking into account equation (32) becomes:

$$\mathbf{j}(s) = -\frac{ie}{\Omega s} f(\mathbf{k}) \, \nabla_{\mathbf{k}} W(\mathbf{k})|_{\mathbf{k}=0} , \tag{36}$$

and returning to the original t-variable

$$\mathbf{j}(t) = en \sum_{m,m'} (\mathbf{R}_{m'} - \mathbf{R}_m) W_{m,m'} , \tag{37}$$

where for $f(0)$ the total number of the carriers in the system, $N = \Sigma_m f_m$, has been substituted. As expected, the final expression for the current density is time-independent. The simplicity of (37) implies that in the special case of periodic systems the CPU charge is reduced to few seconds.

4. Current-field and conductivity-field characteristics - results and discussion

The numerical model presented in the previous section has been implemented over ten years ago by Bottger and co-workers [13-15]. These early works describe rather preliminary results, limited to an extremely low range of the system parameters. In particular, in [13] only a special case of highly diluted system with no on-diagonal disorder is considered, and totally random but spatially uniform on the macroscopic scale distributions of the hopping centres is used. The results of [13] suggest that the differential conductivity σ decreases (down to its negative values) with increasing external field E in the low-field region, whereas in the high-field region the conductivity rapidly increases with increasing field, in agreement with the predictions of the effective medium theory [1]. Such a field dependence of the conductivity is quite different from the conductivity field-dependence in systems with translational symmetry, where σ increases monotonously with increasing field. We have performed extensive calculations in order to study the transition between the two types of the current-field characteristics (Sections 4.1 to 4.3). Furthermore, the influence of the degree of the macroscopic-scale non-uniformity of the centre spatial distribution was investigated (Sec. 4.4).

4.1. The influence of the degree of the off-diagonal disorder

In order to investigate the influence of the off-diagonal disorder on the current-field characteristics, the calculations have been performed for the sequence of the centre distributions obtained as distorted simple-cubic lattices. In particular, the nodal positions were shifted at random within a cube of the edge equal to pa, where a is the cubic lattice constant, and $p = 0.1, 0.2,..., 0.9, 1.0$. Figure 1 shows the current-field characteristics calculated for systems with no on-diagonal disorder, for various degrees of the off-diagonal disorder, and for various dilutions α, where α is defined as the ratio of the average distance between centres to the centre localisation radius. Figure 2 shows the corresponding field dependencies of the differential conductivity. In both Figures the normalised field E' is defined as $E' = qE/2\alpha kT$. As it is seen, although the influence of increasing off-diagonal disorder (increase of p) is qualitatively similar for each dilution, there are significant quantitative differences. In strongly diluted systems the current values increase by several orders of magnitude for p increasing from 0 to 1. Such a behaviour is related to the fact, that in more distorted systems the carriers find more easily an extremely effective percolation cluster which dominates all other paths. In dense systems the dispersion between the

conductivities of different current paths is lower, and the changes of the current values in the function of p in much smaller. The plots of the differential conductivity (Figure 2) reveal the appearance of the conductivity minima for sufficiently disordered systems. At given dilution α the minimum appears at higher fields in more disordered samples (greater p), whereas at fixed value of the p parameter the field corresponding to the conductivity minimum is higher for less diluted centre distributions.

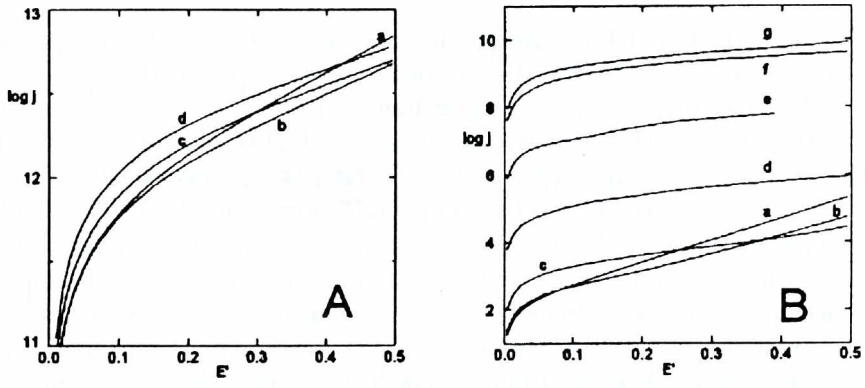

Figure 1. Current-field characteristics calculated for systems with no on-diagonal disorder for various degrees p of the off-diagonal disorder, and for various dilutions . A: $\alpha = 5.0$; curve a: centres in nodal positions of a simple cubic lattice ($p = 0$); curve b: $p = 0.5$; curve c: $p = 1.0$; curve d: totally random centre distribution; B: $\alpha = 15.0$; curve a: $p = 0$; curve b: $p = 0.2$; curve c: $p = 0.4$; curve d: $p = 0.6$; curve e: $p = 0.8$; curve f: $p = 1.0$; curve g: totally random centre distribution.

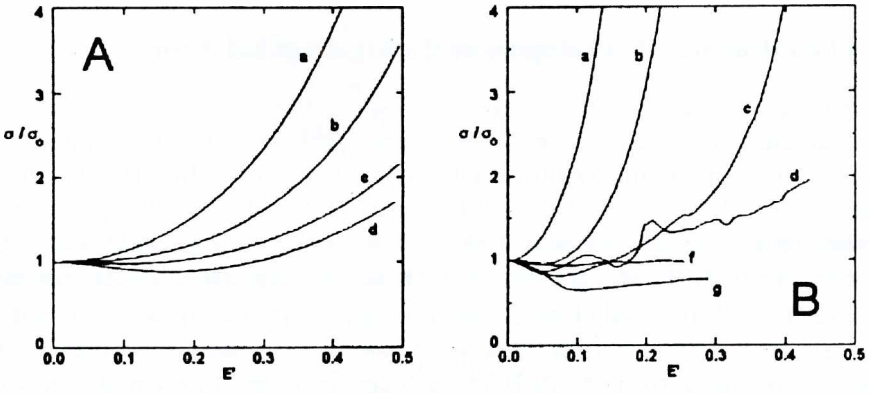

Figure 2. Field dependence of the differential conductivity calculated for the curves of Figure 1. A: $\alpha = 5.0$; B: $\alpha = 15.0$.

4.2. The influence of the system dilution

Current-field characteristics calculated for regular systems (simple cubic lattice) in their dependence on the dilution are shown in Figure 3, whereas the corresponding conductivity-field characteristics are presented in Figure 4. At low fields the Ohm

law is obeyed, and the extension of the ohmic range shrinks on increasing α. The values of fields, at which the conductivity deviates by 1% from its values at $E = 0$ are shown in Figure 6, curve a. In the medium-, and high-field region the current is proportional to $\exp(aE)$ (Figure 3A), and the coefficient a strongly depends on the system dilution. The extension of the ohmic region in random systems is smaller then in the regular ones for dense distribution of centres, whereas for diluted centre distributions a reversed relation holds (Figure 6). Moreover, on increasing off-diagonal disorder the width of the ohmic region becomes less sensitive to the system dilution. As far as the shape of the current-field characteristics is concerned, in random systems the relation $j \sim \exp(aE)$ is also obeyed in the high field region.

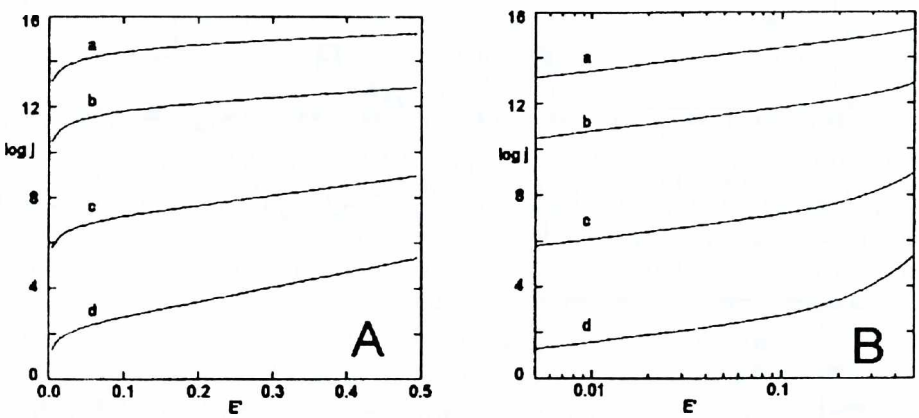

Figure 3. Current-field characteristics for regular (simple cubic lattice) hopping centre distribution in their dependence on dilution . A: lin-log scale; B log-log scale. Curves a: α = 2.5; curves b: α = 5.0; curves c: α = 10.0; curves d: α = 15.0.

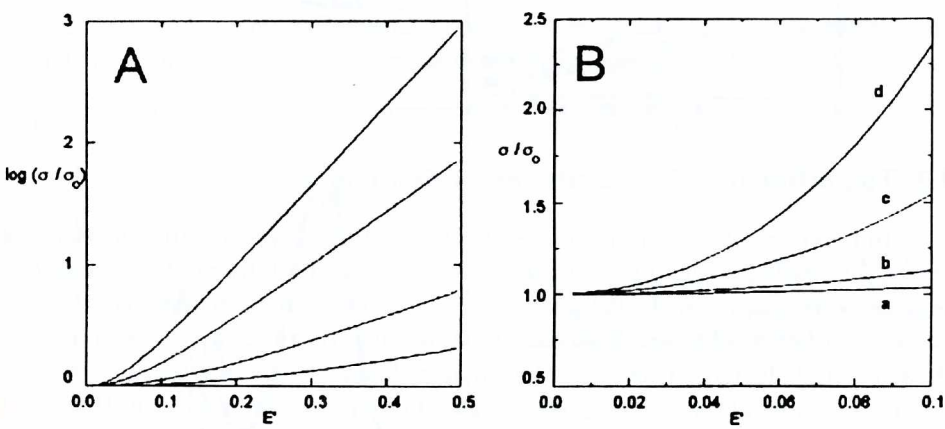

Figure 4. Field dependence of the differential conductivity calculated from characteristics of Figure 3. Curves a: α = 2.5; curves b: α = 5.0; curves c: α = 10.0; curves d: α = 15.0.

However, in contradistinction to the regular centre distribution the *a* coefficient shows rather marginal dependence on α (Figure 5A). Figure 5B shows the appearance of the differential conductivity minimum in sufficiently diluted samples (. Figure 2).

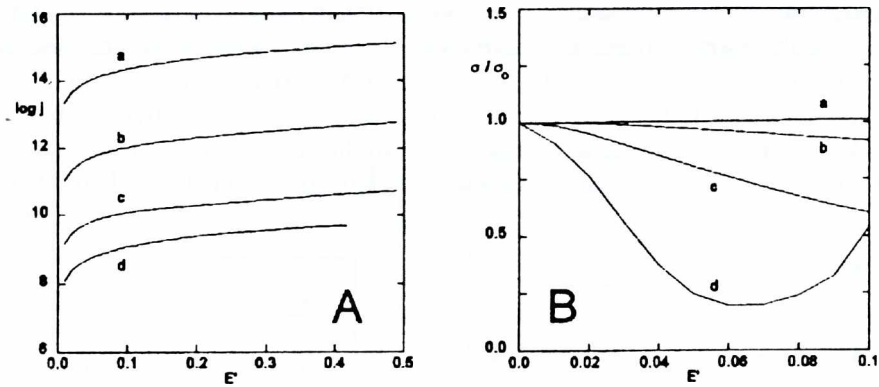

Figure 5. Current-field characteristics (A), and conductivity-field characteristics (B) for random hopping centre distribution in their dependence on dilution . Curves a: α = 2.5; curves b: α = 5.0; curves c: α = 10.0; curves d: α = 15.0.

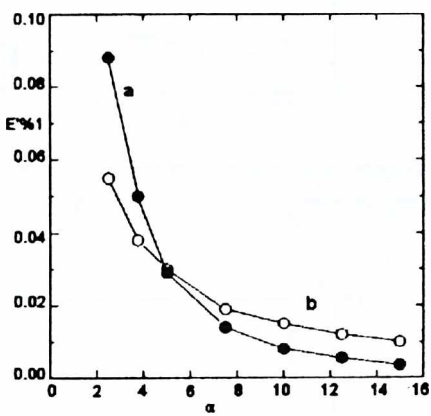

Figure 6. Extension of the ohmic range of the *j-E* characteristics in the function of system dilution . *E'%1* is the field, at which the differential conductivity goes away from its initial value (at *E'* = 0.0) by 1%. Curve a: regular centre distribution, curve b: random centre distribution.

4.3. The influence of the centre co-ordination

In two previous Sections the results obtained for reppresentative model spatial centre distributions (distorted simple cubic lattice, and totally random centre distribution) were discussed. In the present subsection we consider the spatial hopping centre distribution obtained from realistic molecular dynamics structural simulations. As an example let us consider one of the materials revealing a small polaron transport, a binary oxide glass of composition $xV_2O_5(1\text{-}x)P_2O_5$. It is known [19] that in vanadate-phosphate glasses electrons jump between the vanadium ions V^{+4} and V^{+5}. The radial distribution function V-V shows a sharp narrow first peak, the position of which only weakly depends on the glass composition. At the same time the V-V

coordination number depends obviously significantly on the glass stoichiometry. Thus, strong spatial correlations do exist in the glass. No such a correlation appears in random site distribution.

In order to investigate the influence of the average centre co-cordination on the *j-E*, and σ-*E* characteristics we have performed a series of classical molecular dynamics (MD) simulations of the $xV_2O_5(1\text{-}x)P_2O_5$ glass with x = 40%, 50%, 60% and 70%. The MD simulation were performed in isobaric-isoenthalpic (NpH) [20], and microcanonical ensambles for samples containing 2000÷3000 atoms. Interatomic interactions were written in a two-body form (repulsive short range Born-Mayer potential, and long range Coulomb interactions calculated with the aid of the standard Ewald method). The V-O interaction parameters were obtained using the *ab initio* molecular cluster method [21]. Other interaction parameters were taken from [22]. A typical thermal history of the MD-simulated glass consisted in: 1. preparation of well equilibrated melt at high temperature (3000K), 2. stepwise cooling down to 300K, passing equilibrium states at 2000K and 1000K. At each temperature the system was thermalised during $2\div4\cdot10^4$ femptosecond time-steps, whereas the structural information was collected during further $1\div2\cdot10^4$ time-steps. The V-V radial distribution functions for x = 40%, 50%, 60% and 70% are shown in Figure 7. The corresponding V-V coordination numbers are 2.5, 3.1, 3.6, and 4.2, respectively. The final equilibrium distributions of vanadium ions in the glass were then used to calculate the *j-E*, and σ-*E* curves. Within the present model the experimental field dependences of the normal conductivity (*j/E*) are well reproduced for $\alpha = 2.5\div3.0$. Note, that the value of α determined from the AC measurements [19, 23] is about 2.75. Thus, since the average distance between hopping centres (vanadium ions) is almost the same for each x, and only the average centre co-ordination is x-dependent, the dependence of the *j-E* characteristics on the vanadium-phosphate glass stoichiometry can be explained in terms of the variations of the average V-V co-ordination.

Figure 8 shows the differential conductivitiy in its dependence the applied external field for two values of , both much higher then in $xV_2O_5(1\text{-}x)P_2O_5$ glasses,

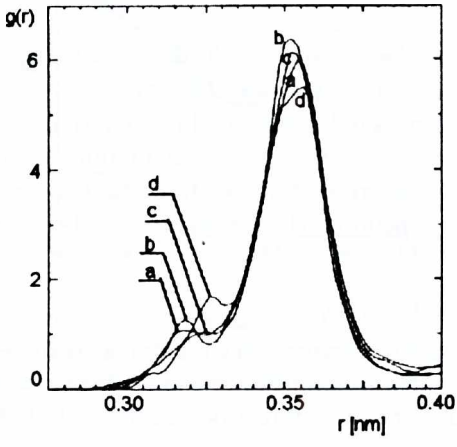

Figure 7. The first peak of the V-V pair radial distribution function for $xV_2O_5(1\text{-}x)P_2O_5$ glasses. Curve a: x = 70%, curve b: x = 60%; curve c: x = 50%; curve d: x = 40%.

for various average centre co-ordinations. It means that the curves in Figure 8 do not correspond any more to the real vanadium-phosphate glass, but rather to a model glass-like spatial distributions of centres, characterised by an approximately constant inter centre distance with various average co-ordinations. As it is seen, the conductivity minima can readily appear in glassy systems even with marginal dispersion in inter centre distances. The minima are deeper for low co-ordination systems, and the depth decreases with increasing value of the ratio between the average inter centre distance and the centre localisation radius. For sufficiently dense systems (small enough) the conductivity minima are absent, and the conductivity increases monotoneously with the field for each x. The increase of is then more rapid for highly co-ordination systems than for low co-ordination systems.

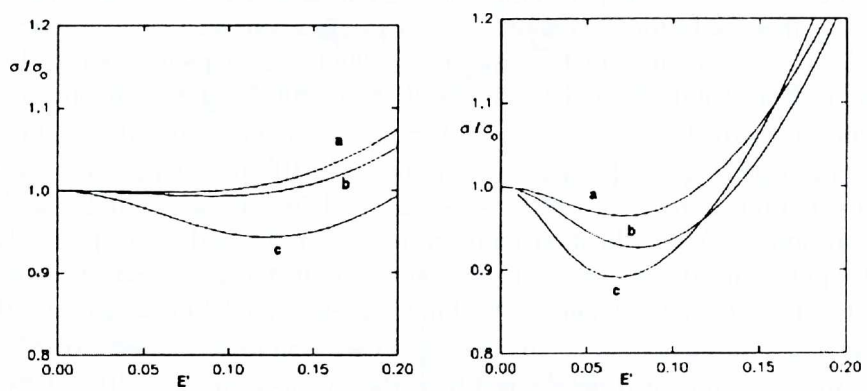

Figure 8. Field dependencies of normalised differential conductivity in their dependence on the avarage co-ordination number and on the system dilution . The conductivities calculated for the centre distribution is topologically equal to the distribution of vanadium atoms in MD simulated samples. Figure A: $\alpha = 5.0$; Figure B: $\alpha = 10.0$. Curves a: average centre co-ordination 4.2; curves b: 3.6; curves c: 3.1.

4.4. The influence of the macroscopic-scale spatial non-uniformity of the centre density

An exponential dependence of the hop probability on the distance between the neighbouring centres should lead also to a strong influence of the macroscopic-scale variations of the centre density on the current-field, and conductivity-field characteristics. In order to investigate this phenomenon a series of calculations for exponentially changing concentration of centres were performed. In particular, the total centre concentration N_h was assumed to depend on the distance from the injecting contact as

$$N_h \propto \exp(-x/D), \tag{38}$$

whereas the energetic centre distribution $f(\varepsilon)$ was constant over the layer thickness. Figure 9 shows the current field characteristics of samples containing always the same number of states (1000), distributed along the field direction according to (38) for

various degrees of spatial non-uniformity L/D, where L is the layer thickness. The L/D ratio ranged from 0.0 (spatially uniform system) to 3.0, and the calculations were repeated for various dilutions . The curves obtained for spatially non-uniform layers with $L/D = 1.0 \div 3.0$, for sufficiently high dilutions (Figures 9B, 9C, 9D) have an N-like shape, *i.e.* the current reaches its maximum value at relatively low fields (Figure 11, curves a, and b), then decreases to its minimum value, and finally increases exponentially at higher fields. Both the position and the depth of the current minima depend strongly on the degree of the spatial non-uniformity of the centre concentration. With increasing L/D ratio the minimum values of the current become lower, and appear at higher fields (Figure 11, curves c-e). Figure 10 shows differential conductivity $\sigma(E')$, normalised to $\sigma(E' = 0)$, calculated from the characteristics of Figure 9. As it is seen, the curves corresponding to $L/D \geq 1.0$ are all almost identical each to other, at least for sufficiently diluted systems. It means that in relatively diluted systems the relative changes of the differential conductivity do not depend

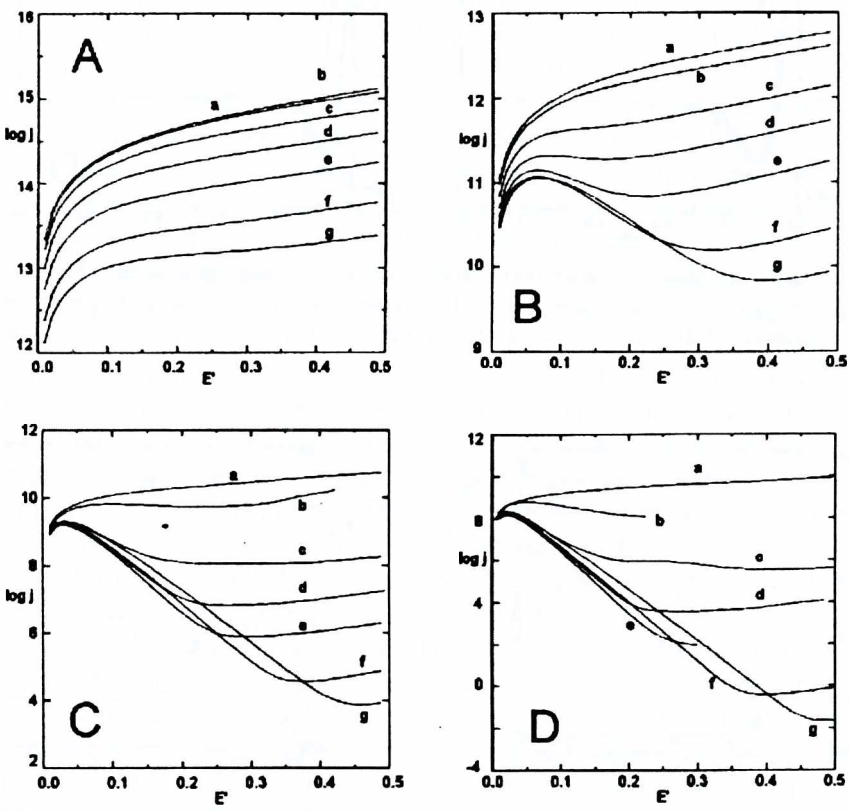

Figure 9. Current-field characteristics calculated for various layer non-uniformity parameters L/D. Figure A: $\alpha = 2.5$; Figure B: $\alpha = 5.0$; Figure C: $\alpha = 10.0$; Figure D: $\alpha = 15.0$. Curves a: $L/D = 0.0$; curves b: $L/D = 0.5$; curves c: $L/D = 1.0$; curves d: $L/D = 1.5$; curves e: $L/D = 2.0$; curves f: $L/D = 2.5$; curves g: $L/D = 3.0$.

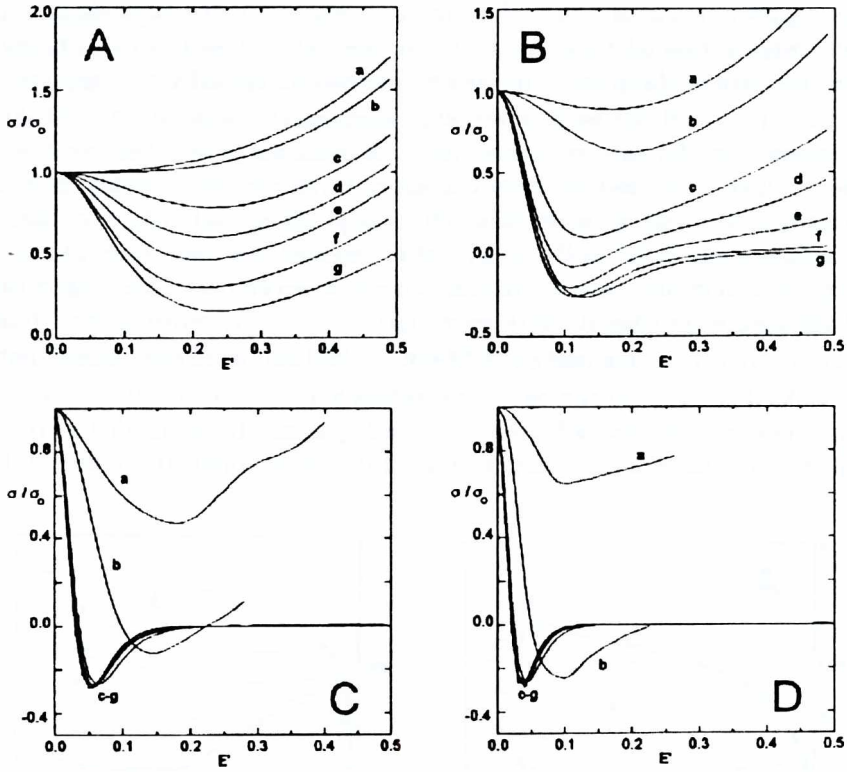

Figure 10. Field dependencies of the differential conductivity calculated for systems of Figure 9. Figure A: $\alpha = 2.5$; Figure B: $\alpha = 5.0$; Figure C: $\alpha = 10.0$; Figure D: $\alpha = 15.0$. Curves a: $L/D = 0.0$; curves b: $L/D = 0.5$; curves c: $L/D = 1.0$; curves d: $L/D = 1.5$; curves e: $L/D = 2.0$; curves f: $L/D = 2.5$; curves g: $L/D = 3.0$.

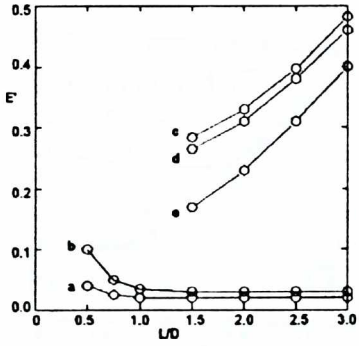

Figure 11. The dependence of $E'_{max\text{-}cur}$ (a-b) and $E'_{min\text{-}cur}$ (c-e) on the layer non-uniformity parameter L/D. Curve a: $\alpha = 15.0$; curve b: $\alpha = 10.0$; curve c: $\alpha = 15.0$; curve d: $\alpha = 10.0$; curve e: $\alpha = 5.0$.

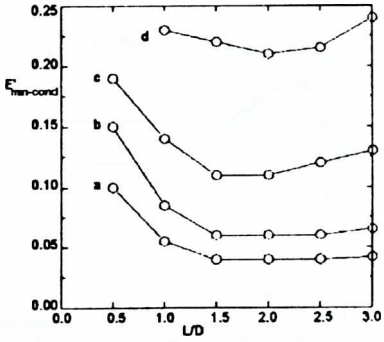

Figure 12. The dependence of $E'_{min\text{-}cond}$ on the layer non-uniformity parameter L/D. Curve a: $\alpha = 15.0$; curve b: $\alpha = 10.0$; curve c: $\alpha = 5.0$; curve d: $\alpha = 2.5$.

significantly on the degree of the spatial non-uniformity of the layer L/D, if only the latter exceeds some critical value, and the dependence of σ on E' assumes an universal characteristic shape. The minimal (and negative for sufficiently diluted systems) value of the conductivity, weakly dependent on the L/D ratio, appears at a field E'_{min} dependent on the system dilution α (Figure 12). With further increase of the field the conductivity increases, and at E'_{sat} assumes a small positive saturation value, constant over a wide range of external fields. E'_{sat} only weakly depends on the non-uniformity parameter L/D for a fixed value of the dilution α. On the other hand E'_{sat} depends significantly on α (E'_{sat} amounts to 0.2, and 0.14 for α equal to 10.0, and 15.0, respectively).

The existence of a wide field range of a negative differential conductivity in sufficiently diluted spatially non-uniform systems is the most important result of the present section. The effect is absent in spatially uniform systems, where the conductivity has a minimum, but its values remain positive in the whole field range. In order to explain the difference between uniform, and non-uniform systems, the histograms of the average occupation probabilities $P(i)$, $i = 1,...,10$ in ten subsequent slices of the layer along the field direction were plotted. Figures 13-15 show such histograms in their dependence on E' for $L/D = 0.0$, 1.5 i 3.0 in a strongly diluted sample with = 15.0. The histograms A in Figures 13-15 correspond to a very low field strength, $E' = 0.005$. For the spatially uniform layers the average occupation numbers in the successive $L/10$ - thick slices do not differ significantly from their equilibrium values at zero field, and the field $E' = 0.005$ falls well into the ohmic region (Figure 13A). However, for the non-uniformity parameter L/D equal to 1.5 and 3.0 (Figures 14A, and 15A, respectively) the value $E' = 0.005$ lays in the non-ohmic region, and the deviations from the equilibrium zero-field occupation $n = 0.5$ are significant. Nowhere over the layer thickness the average occupation is close to 1.0, and the value $E' = 0.005$ falls into the region of positive differential conductivity for all values of L/D. Increasing field leads to remarkable changes in $P(i)$ probabilities. In particular, within the sample emerges a region with the average occupation probability close to 1.0. The field interval in which only few of the $P(i)$'s effectively approaches this maximum value corresponds to a subohmic portion of each current-field characteristic, *i.e.* to the decay of differential conductivity to zero. For higher fields the extension of the region with $P(i)$ close to 1 augments, for more non-uniform structures covering practically the whole bulk of the sample. This field range corresponds to the portions of decreasing current with increasing field, *i.e.* to the regions of the negative differential conductivity. Finally, the increasing field is again able to enforce the effective carrier motion, and the current begins to increase slightly, so that the conductivity assumes small positive values: in this field interval the spatial extention of the $P(i)=1$ region begins to shrink. The exponential conductivity increase at high fields, expected for macroscopically uniform systems [24-29], is not observed for the investigated non-uniform systems. It means, that the sample non-uniformity shifts the region of the exponential current increase to the fields values, which could not be consistent with the assumption of constant carrier concentration.

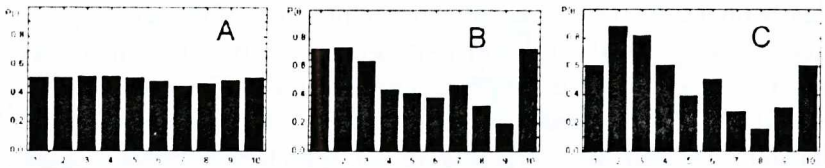

Figure 13. Histograms of the average site occupation in ten subsequeunt slices of the spatially uniform layer of thickness L. Figure A: $E' = 0.005$; Figures B,C: $E' = 0.5$ for two different random distributions of hopping centres.

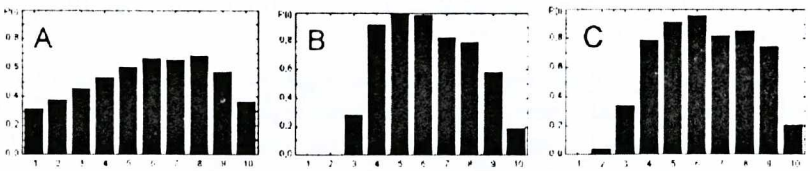

Figure 14. Histograms of the average site occupation in ten subsequeunt slices of the spatially non-uniform layer of thickness L and the non-uniformity parameter $L/D = 1.5$. Figure A: $E' = 0.005$; Figure B: $E' = 0.2$; Figure C: $E' = 0.4$.

Figure 15. Histograms of the average site occupation in ten subsequeunt slices of the spatially non-uniform layer of thickness L and the non-uniformity parameter $L/D = 3.0$. Figure A: $E' = 0.005$; Figure B: $E' = 0.2$; Figure C: $E' = 0.8$.

5. Concluding remarks

The model of hopping transport reminded in Sections 2 and 3 is rather difficult to be treated numerically. In order to obtain fully realistic results one should perform calculations involving - as results from our tests - at least 10^4 hopping centers in the simulation box. For such a number of centres one could claim to obtain the results free not only of box-size effects, but also independent of the random generation of the localised centre positions. Unfortunately, the increased remarkably number of sites in the simulation box, in addition to increase strongly the difficulty of operating numerical methods, would demand extremely long CPU times, and thus such calculations are practically impossible. We think, however, that even somewhat oversimplified numerical results, obtained for merely 10^3 hopping sites, reveal qualitative behaviours of real physical systems.

Acknowledgement

The opportunity to perform our numerical calculations at the T.A.S.K. Computer Centre (Gdańsk, Poland), and at CIC (Camerino, Italy) is kindly acknowledged. The work has been partially sponsored by CNR, grant 96.00844.ST76.

References

[1] Bottger H and Bryksin V V 1985 *Hopping conduction in Solids* Academie-Verlag Berlin

[2] Fritzsche H and Pollak M 1990 *Hopping and Related Phenomena* World Scientific, Singapore

[3] Pollak M and Shklovskii B 1991 *Hopping Transport in Solids* North-Holland

[4] Bottger H and Bryksin V V 1980 *Phil. Mag.* **B42** 297

[5] Broadbent S R and Hammersley J M 1957 *Proc. Cambridge Phil. Soc.* **53** 628

[6] Klein W and Kinzel W 1981 *J. Phys.* **A14** L 405

[7] Redner S 1982 *Phys. Rev.* **B25** 5646

[8] Pollak M and Riess I 1976 *J. Phys.* **C9** 2339

[9] van der Meer M, Schuchardt R and Keiper R 1982 *phys. stat. sol.* (b) **110** 571

[10] Bottger H and Bryksin V V 1979 *phys. stat. sol.* (b) **96** 219

[11] Kirkpatrick S 1973 *Revs. Mod. Phys.* **45** 574

[12] Bryksin V V and Yashin G Yu 1981 *Fiz. tverd. Tela* **23** 3063

[13] Bottger H and Wegener D 1984 *Phil. Mag.* **B50** 409

[14] Bottger H, Szyler P and Wegener D 1985 *phys. stat. sol.* (b) **128** K179

[15] Bottger H, Szyler P and Wegener D 1986 *phys. stat. sol.* (b) **133** K143

[16] Mancini G and Rybicki J 1992 *J. Phys.* **CM 5** 4475

[17] Mancini G and Rybicki J 1995 *J. Phys.* **CM 7** 8467

[18] Rybicki J and Mancini G 1997 submitted to *J. Phys.* **CM**

[19] Murawski L 1995 *Zesz. Nauk. PG, Fizyka* **29** Gdańsk

[20] Andersen H C 1980 *J. Chem. Phys.* **72** 2384

[21] Takada A, Catlow C R A and Price G D 1995 *J. Phys.* **CM7** 8659; *ibid.* 8659

[22] Abrahamson A A 1969 *Phys. Rev.* **178** 76

[23] Murawski L, Barczyński RJ and Rybicka A 1996 *Proc. Conf. Dielectric and Related Phenomena*, Szczyrk 16-20 Sept. 1996, Poland (in print)

[24] Mott N F 1971 *Phil. Mag.* **24** 911

[25] Apsley N and Hughes H 1975 *Phil. Mag.* **31** 1325

[26] Austin I G and Sayer M 1974 *J. Phys.* **C7** 905

[27] Hill R M 1971 *Phil. Mag.* **24** 1307

[28] Shklovskii I 1972 *Fiz. Tekh. Poluprov.* **6** 2335

[29] Shklovskii I 1976 *Fiz. Tekh. Poluprov.* **10** 1440